Copyright © 2022 Elsevier Ltd. All rights reserved. This is the accepted manuscript version of an article which has been published in final form at https://doi.org/10.1016/j.energy.2022.124719, made available on this repository under a Creative Commons CC BY-NC-ND attribution licence (https://creativecommons.org/licenses/by-nc-nd/4.0/).

The modeling of transient phase changes of water droplets in flue gas flow in the range of temperatures characteristic of condensing economizer technologies

Gintautas Miliauskas[1], Egidijus Puida[1], Robertas Poškas[2*], Povilas Poškas[2], Algimantas Balčius[1], Hussam Jouhara[3]

[1] *Department of Energy, Kaunas University of Technology, Studentu 56, Kaunas LT-51424, Lithuania*

[2] *Nuclear Engineering Laboratory, Lithuanian Energy Institute, Breslaujos 3, Kaunas LT-44403 Kaunas, Lithuania*

[3] *Heat Pipe and Thermal Management Research Group, College of Engineering, Design and Physical Sciences, Institute of Energy Futures, Brunel University London, UB8 3PH UK*

**Corresponding author: Robertas.Poskas@lei.lt , Tel.: +370 37 401893. Postal address: Lithuanian Energy Institute, Breslaujos 3, LT-44403 Kaunas, Lithuania*

ABSTRACT

Heat transfer and phase change processes of water droplets in humid air flow were investigated by performing experiments and numerical simulations of heat recovery from biofuel exhaust gas at 40–250 ºC, which is characteristic for condensing heat exchangers. Compared to the experiments, the numerical investigation was performed within a wider range of boundary conditions considering droplet dispersity and flue gas parameters. The reliability of the simulation was justified through the coincidence between the calculated temperature of the equilibrium evaporation of droplets (convection heat transfer) in humid air and the wet-bulb thermometer temperature. In the case of droplet combined heating (radiation and convection), the methodology was justified by coincidence between the calculated equilibrium evaporation velocity and experimental results obtained by other authors. When the temperature of the radiation source is lower than 150 ºC, the vapor flows calculated at the surface of the droplets in equilibrium evaporation in the cases of combined heating and convective heat transfer differ by about 0.1 percent, therefore, the radiation influence can be neglected. Based on the results obtained in the investigation of the droplet's phase changes, the work includes practical recommendations for technological water injection to ensure optimal heat recovery from wet exhaust gas in condensing economizers.

Keywords: water droplet, humid gas flow, complex transfer processes, condensation, evaporation, numerical modeling

Nomenclature

a	[m^2/s]	thermal diffusivity
B_M	[-]	Spalding mass transfer parameter
B_T	[-]	Spalding heat transfer parameter
c_p	[J/(kg K)]	mass specific heat
C_l	[-]	droplet drag coefficient
D	[m^2/s]	mass diffusivity
Fo	[-]	Fourier number
k_{ef}	[-]	effective conductivity parameter
g_v	[kg/s]	vapor mass flux
L	[J/kg]	latent heat of evaporation
m_v	[kg/(m^{2}s)]	vapor mass flux density
M	[kg/kmol]	molecular mass
n	[-]	number of the term in infinitive sum
Nu	[-]	Nusselt number
p	[Pa]	pressure

p_b	[Pa]	barometrical pressure
P		symbol of free parameter in heat-mass transfer
Pr	[-]	Prandtl number
r	[m]	radial coordinate
R	[m]	radius of a droplet
Re	[-]	Reynolds number
$R\mu$	[J/(kmol K)]	universal gas constant
R_g	[J/(kg K)]	gas constant
R_v	[J/(kg K)]	vapor constant
q	[W/m^2]	is heat flux
S	[m^2]	area of a droplet surface
Sh	[-]	Sherwood number
Sc	[-]	Schmidt number
t	[°C]	temperature
T	[K]	temperature
w	[m/s]	velocity
w_{lg}	[m/s]	droplet slip velocity in to gas
X_v	[-]	vapor volumetric fraction
Y_v	[-]	vapor mass fraction

Greek symbols

δ	[%]	relative error
η	[-]	non-dimensional radial coordinate
λ	[W/(m K)]	thermal conductivity
ρ	[kg/m^3]	density
τ	[s]	time
τ_r	[s]	point in time, when temperature field with a negative gradient is formed in the droplet
μ	[Pa s]	dynamics viscosity
φ	[%]	relative humidity

Subscripts

a	atmospherically
c	convective
co	condensation
dp	dew point
dr	dry
e	equilibrium evaporation
ek	equivalent
eks	experimental
f	phase change
g	gas
i	time index in digital scheme
I	index of control time
I_f	index of droplet evaporation time end point $\tau=\tau_f$
it	number of iteration
IT	is number of final iteration of iterative cycle
j	index of radial coordinate in digital scheme
J	index of a droplet surface

l	liquid
m	mass average
r	radiative
R	droplet surface
s	saturation
v	vapor
vg	vapor gas mixture
wb	wet-bulb thermometer
Σ	total
0	initial
∞	far from a droplet

1. Introduction

A basic element in the combustion of liquid fuels in engines and boilers, in flue gas cleaning and heat recovery from them, air conditioning and other modern technologies is the process of liquid evaporation and vapor condensation [1–6] et al. The applications of liquid injection (usually liquid fuel and water) in the technological practices means that the heat and mass transfer in droplets must be thoroughly analyzed over a wide range of boundary conditions. The heat and mass transfer processes in liquid droplets have been investigated for more than a hundred years [7, 8]; however, the constant need to upgrade liquid dispersion-based modern technologies and make them more effective ensures constant attention to the so-called "droplet" investigation [9].

Liquid dispersed to droplets attains the boundary conditions closer to those of nanotechnologies, and the interaction between the processes of combined heat and mass transfer then becomes very intensive. The balance between the heat flux that the droplet receives and the phase change heat flux that takes place in the evaporation process is achieved at a certain temperature T_e characteristic of equilibrium liquid evaporation, which is lower than the temperature T_s of the liquid in the saturation state. The Stefan flow, which always accompanies phase changes, is considered to be the defining factor for the interaction between external processes of convective transfer in droplets [10]. In the droplet, during the interaction of the processes of combined heat transfer, the main factors are radiation absorption in a semi-transparent droplet and liquid circulation within the droplet [9, 11]. Thermal radiation absorption in a semi-transparent droplet is accompanied by numerous light spectral effects [12], which are defined by the complex refractive index of the liquid. The complex refractive index of water undergoes very intense and clearly non-linear changes within the radiation spectrum [13], and therefore, the absorption of the radiation flux in droplets is uneven [14].

The methods and results of experimental and numerical investigations of heat and mass transfer in liquid sprays and droplets are summarized systematically up to 2014 in works [7, 9]. The key findings of the investigation of the interactions between liquid droplet transfer processes are the influence of the Stefan flow on phase changes and convective processes in heat transfer, the development of a reliable methodology for numerical evaluation (which is based on the Spalding theory for heat and mass transfer parameters), and the development of the methodology for the numerical simulation of combined heat and mass transfer in semi-transparent droplets (the methodology is based on spectral radiation models and is essential in the definition of transitional phase change processes in droplets). In the current stage of "droplet" investigation, methods for droplet numerical simulation must be improved [15–22] (one should concentrate on transition phase change regimes and interaction between combined transfer processes).

The credibility of the results obtained during the numerical simulation of heat and mass transfer is ensured by comparison of the simulation results and the experimental results of the droplet evaporation rate, which is so important to liquid spraying technologies. In [23] scientists experimentally measured the equilibrium evaporation rate of a large water droplet (R≡0.5–1.6 mm) heating up in

atmospheric air of a high temperature (t_g≡405–860 ºC) under the conditions of combined heating (the vapor flux was assumed to be equal to the measured flow rate of the water supplied to the droplet through the capillary when the temperatures of the droplet and the supplied water as well as the illuminated projection of the droplet on a screen became steady). The droplet was supplied with heat by weak external convection (caused by the suction of the vapor and air mixture when w_g=0.01 m/s [23]) and by radiation from the iron wall that was restricting the air. The results of the experiments conducted justified the fact that the vapor flux, in the case of combined heating, at the surface of the water droplet undergoing equilibrium evaporation, is not only defined by the temperature and humidity of the gas, but is also influenced by the dispersity of the droplet.

The temperature of humid flue gas after the biofuel boiler can range from 150 ºC to 250 ºC depending on the boiler's design and the biofuel type [24–27]. Before the water spray, the flue gas should be cooled down before the condensing economizer to a temperature similar to the dew point temperature (flue gas is additionally humidified and the dew point temperature increases) so that the technological process of heat recovery can be efficient.

The complex experimental and numerical investigation of water droplet heat and mass transfer presented concentrates on the boundary conditions characteristic of heat recovery from biofuel exhaust gas in condensing economizers. The influence of air flow humidification on the thermal state and phase changes of a water droplet was experimentally investigated in [28]. The air flow was heated to 140 ºC and additionally humidified to Xv = 0.3. The present work reports a numerical simulation of the heating and phase changes of dispersed water droplets in the flow of biofuel exhaust gas, cleaned of solid particles, and preheated to 250 ºC and humidified to X_v = 0.5.

2. Methodology

The complex experimental and numerical investigation performed for water droplet combined heat and mass transfer processes in wet flue gas flows are congruent to the worldwide investigation of "single liquid droplet" transfer processes. This has gained popularity because the results obtained during the investigation of heat transfer and phase changes in a single droplet are the cornerstone for the investigation of two-phase flows with dispersed liquids [29].

Phase change processes of water droplets in the flue gas flow were modeled using various boundary conditions of heat and mass transfer in the condensing economizer ($2R$ = 50-500 μm, t_g = 40–250 ºC, X_v= 0.07–0.5). The boundary conditions of the experiments performed in [23, 28] were also reproduced numerically.

2.1. The model of heat and mass transfer in a droplet

The water droplet heat and mass transfer processes are modeled using QBASIC with the original numerical investigation software LASAS developed by Kaunas University of Technology's Department of Energy (author G. Miliauskas). The numerical iterative scheme defining the average instantaneous temperature of the droplet's surface and working according to the fastest convergence method is based on the energy balance of thermal flows moving towards and away from the droplet's surface [16]:

$$\vec{q}_{c,g}(\tau) + \vec{q}_{c,l}(\tau) + \left[\vec{q}_{r,g}(\tau) - \vec{q}_{r,l}(\tau)\right] + \vec{q}_f(\tau) = 0\,. \quad (1)$$

Equation (1) is too formal to be used directly to draw a numerical scheme and define the temporal function of the temperature of the droplet's surface. Yet, equation (1) shows a close connection between the droplet's phase changes and its heat transfer processes, as well as justifying the need to consider the interaction between combined transfer processes. Due to the intense interaction of the heat and mass transfer processes, the state of a droplet in the equilibrium evaporation regime is different from that of a large volume of liquid. A large volume of liquid warms up to the saturation temperature T_s and boils. The droplet evaporates at a lower temperature T_e and the liquid within it does not boil. At

the end of the transition evaporation region, the water droplet reaches the thermal state characteristic of equilibrium evaporation. The condensation regime takes place when the initial temperature $T_{l,0}$ of the droplet is lower than the dew point temperature T_{dp}. An explosive evaporation of the droplet does not happen.

Heat and mass transfer processes of water injected into the biofuel flue gas flow are analyzed in the cycle of phase change regimes:

$$\tau \equiv 0 \to \tau_{co} \to \tau_r \to \tau_e \to \tau_f \tag{2a}$$

The cycle of phase change regimes (2a) and its incipience (τ=0) coincide with the formation of technological droplets [30]. The variation of phase change regimes is defined by the time end points $\tau=\tau_{co}$ and $\tau=\tau_e$ of condensation and transient evaporation regimes, respectively. The end of the cycle in (2a) is defined by the droplet evaporation time end point $\tau=\tau_f$. The formal equation of the droplet energy balance (1) assumes the specific form in respective regimes.

The condensation regime continues until the droplet's surface heats up to the dew point temperature T_{dp}. Equation (2b) assumes that all heat supplied to the droplet in the condensation regime heats the water:

$$q_{c,l}(0 \le \tau < \tau_{co}) = q_{c,g}(\tau) + q_f(\tau); \quad q_{c,l}(\tau = \tau_{co}) \ = q_{c,g}(\tau_{co}) \ . \tag{2b}$$

In the transition evaporation regime, the water is heated and evaporates. Equation (2c) then assumes that the phase change heat flux is defined by the difference between internal and external convection flows:

$$q_f(\tau_{co} < \tau < \tau_r) = q_{c,g}(\tau) - q_{c,l}(\tau); \ q_f(\tau = \tau_r) = q_{c,g}(\tau_r) \ . \tag{2c}$$

During the transient evaporation regime, a temperature field with a negative gradient is formed in the semitransparent droplet under the action of the absorbed radiation flux. From this time τ_r, the heat flux absorbed in the water droplet gradually becomes a part of the water surface evaporation process. Equation (2d) takes into account that the radiation flux in the evaporation process is defined by internal heat convection flow in the droplet:

$$q_f(\tau_r < \tau < \tau_e) = q_{c,g}(\tau) + q_{c,l}(\tau); \ q_f(\tau = \tau_e) = q_{c,g}(\tau_e) + q_{r,l}(\tau_e) \ . \tag{2d}$$

At the starting time point τ_e of equilibrium evaporation, the whole radiation flux absorbed in the droplet takes place in the evaporation process. Equation (2e) considers that the droplet can cool down in the equilibrium evaporation regime:

$$q_f(\tau > \tau_e) = q_{c,g}(\tau) + q_{c,l}(\tau); \ q_{c,l}(\tau > \tau_e) = q_{r,l}(\tau) - \frac{1}{3}\rho_l c_{p,l} R \frac{dT_{l,m}}{d\tau} . \tag{2e}$$

In such a case, the evaporation process is enhanced by the heat flux proportional to the change in the droplet's enthalpy. This heat flux gets to the droplet's surface by internal convection together with the absorbed radiation flux. The thermal state of a non-isothermal droplet is defined by its mass average temperature. The change in such a temperature in the cycle of phase change regimes (2a) is described based on the function $T(r,\tau)$ of the transient temperature field:

$$T_{l,m}(\tau) = \frac{\int_0^R \rho_l(\tau,r) c_{p,l}(\tau,r) T(\tau,r) r^3 dr}{\int_0^R \rho_l(\tau,r) c_{p,l}(\tau,r) r^3 dr}. \tag{3}$$

The temperature field of the droplet, as in [5], is described based on an integral model [31] of combined heat dissipation in a semi-transparent sphere by radiation and conduction. Yet, it also includes the

effective thermal conductivity coefficient $\lambda_{ef}=\lambda_l k_{\mathrm{ef}}$ of water and, hence, additionally considers the forced water circulation in a droplet [31]:

$$T(r,\tau) = T_R(\tau) + \frac{2}{r}\sum_{n=1}^{\infty} sin\frac{n\pi r}{R}\int_0^{\tau} f_n\, exp\left[-\frac{\lambda_{ef}}{\rho_l c_{p,l}}\left(\frac{n\pi}{R}\right)^2(\tau-\tau_*)\right]d\tau_* \tag{4a}$$

$$f_n = \frac{(-1)^n R}{n\pi}\frac{dT_R}{d\tau} + \frac{1}{R\rho_l c_{p,l}}\int_0^R \left(sin\frac{n\pi r_*}{R} - \frac{n\pi r_*}{R}cos\frac{n\pi r_*}{R}\right) q_r dr \tag{4b}$$

The effective conductivity parameter k_{ef} is defined based on recommendations of work [32]. The influence of the absorbed radiation flux is assessed in equation (4a) by the function f_n (4b) of the n^{th} term of the infinite sum.

The local radiation flux in the semi-transparent droplet is defined according to a spectral model developed based on geometrical optics [31]. The complex refractive index of water is selected according to the data from work [13]. The external and internal reflection of the light beam on the droplet's surface, refraction in contact with water, and the influence of the Brewster's angle in the spectrum of infrared rays are defined according to recommendations of work [12]. In the case of convective heating, the radiation flux q_r equals zero in equation (4b). The differential equation for phase change dynamics describes the change in the droplet's mass and volume [12]:

$$\frac{d}{d\tau}\left[\frac{4}{3}\pi\rho_l R^3\right] = -g_v = -4\pi R^2 m_v\,. \tag{5}$$

The convective heat and mass transfer of the droplet is described based on the Reynolds analogy. The Nusselt number and the Sherwood number are then described based on the justified correlation of Clift et al. [33]:

$$\mathrm{Nu} = 1 + (1+\mathrm{RePr})^{\frac{1}{3}} f(Re), \tag{6a}$$

$$\mathrm{Sh} = 1 + (1+\mathrm{RePr})^{\frac{1}{3}} f(Re), \tag{6b}$$

$$f(\mathrm{Re}\le 1) = 1,\quad f(1<\mathrm{Re}\le 400) = \mathrm{Re}^{0.077};\ \mathrm{Re} = 2R\frac{\rho_g|w_{lg}|}{\mu_{vg}}. \tag{6c}$$

Correlations (6a) and (6b) summarize the results of droplet convective heat and mass transfer studies with greater than 97 percent confidence. The influence of the Stefan flow, which always accompanies the droplet phase changes, is evaluated by functions of Spalding's heat and mass numbers, B_T and B_M, respectively, following the recommendations in [32]:

$$q_{c,g} = \mathrm{Nu}_f\frac{\lambda_{vg}}{2R}\left(T_g - T_R\right);\ \mathrm{Nu}_f = 2\frac{ln(1+B_T)}{B_T} + \frac{\mathrm{Nu}-2}{(1+B_T)^{0.7}};\ B_T = c_{p,vg}\frac{T_g-T_R}{L}\frac{q_f}{q_{c,g}} \tag{7a}$$

$$g_v = 2\pi R\rho_{vg}D_{vg}\mathrm{Sh}_f\, ln(1+B_M);\ \mathrm{Sh}_f = 2 + B_M\frac{\mathrm{Sh}-2}{(1+B_M)^{0.7}\, ln(1+B_M)};\ B_M = \frac{Y_{v,R}-Y_{v,\infty}}{1-Y_{v,R}} \tag{7b}$$

The versatility of the convective heat and mass transfer models (7a and 7b) during the regimes of the droplet's phase change cycle (2a) is ensured because the empirical correlations of Spalding's B_T and B_M numbers consider the changed direction of the vapor flux vector when the condensation regime changes to the evaporation regime [16].

The droplet slip velocity in gas flow is described by the differential equation of motion applying the model provided in [17, 34]:

$$w_{lg} = w_g - w_l, \tag{8a}$$

$$\frac{dw_l}{d\tau} = \frac{3}{16}\frac{\mu_g}{\rho_l}\frac{w_{lg}}{R^2}C_l\,Re_\infty;\ \ \mathrm{Re}_\infty = 2R\frac{\rho_g}{\mu_g}\left|w_{lg}\right| \tag{8b}$$

$$C_l = \frac{24+4.8Re^{0.63}}{(1+B_T)^{0.2}Re}. \tag{8c}$$

The temperature gradient in the droplet is defined based on equation (4) according to Fourier's law of thermal conduction:

$$q_{c,l} = -\lambda_{ef}\frac{\partial T(r,\tau)}{\partial r}\Big|_{r=R}. \tag{9}$$

The complex refractive index of water in the thermal radiation spectrum is finite [13], and therefore the absorption of radiation flux in the surface of the droplet is denied ($q_{r,g}$-$q_{r,l}\approx 0$). The direction of external convection heat flux is defined by the difference between the temperatures of the gas and the droplet surface, assuming that $T_g > T_R$. The vapor flux, which is calculated according to model (7b), has a negative value in the condensation regime and a positive value in the water evaporation regime. The direction of the vector of internal convection heat flux is defined by the gradient of the temperature field in the droplet. Then, the dynamics of the heat flux balance at the droplet surface during the cycle (2a) of phase change regimes is described by the universal equation:

$$\lambda_g^v\frac{\mathrm{Nu}_f}{2R}\left(T_g - T_R\right) - L\frac{\mathrm{Sh}_f}{2R}\rho_{vg}D_{vg}\,ln(1+B_M) = \lambda_{ef}\mathrm{grad}T_R. \tag{10a}$$

The gradient of the temperature field of a droplet is described by the integral equation [31]

$$gradT_R = \frac{2\pi}{R^2}\sum_{n=1}^{\infty}(-1)^n n\int_0^\tau f_n\,exp\left[a_l\left(\frac{n\pi}{R}\right)^2(\tau_* - \tau)\right]d\tau_*. \tag{10b}$$

2.2. Methodology for numerical simulation

Equation (10a) is a transcendental function as the model of the Spalding heat transfer B_T number includes the unknown flux $q_{c,g}$. Furthermore, the local radiation flux can be calculated only when the temperature field of the droplet is known. Therefore, equation (10a) is solved numerically according to an iterative scheme in respect of the surface temperature. In the cycle of the droplet's phase change regimes (2a), control time periods τ_i are set in equal variational steps:

$$\tau_{i=1} = 0;\ \tau_I = \tau_f;\ \ \tau_i = \tau_{i-1} + \Delta\tau\,, \tag{11a}$$

$$\sum_{i=2}^{I_f}(\tau_i - \tau_{i-1}) = \tau_f. \tag{11b}$$

The integer I_f in equation (11b) is selected individually for each simulation case so that at least one hundred of control time periods τ_i could be evaluated during the droplet's transitional phase change regime. In equation (4b) of function f_n, the integral in radial coordinates is defined numerically.The dimensionless radial coordinate $\eta = r/R$ is introduced for this purpose. This radial coordinate ensures a dimensionless unique η=1 beam of the droplet in the whole cycle of the droplet's phase change regimes (2a).

When the integer J=41 is defined [35], control sections described by coordinate η_j are defined in the droplet's beam:

$$\eta_1 = 0;\ \eta_J = 1;\ \eta_{1<j<J} = \eta_{j-1} + \frac{1}{J-1}, \tag{12a}$$

$$\sum_{j=2}^{J}\left(\eta_j-\eta_{j-1}\right)=1. \tag{12b}$$

At each control time point $\tau_{I=1<i<If}$ (starting with $\tau_{i=2}$), the following iterative cycle was performed:

$$it=1\div IT \tag{13}$$

In this iterative cycle (13), equation (10) is minimized numerically by the fastest convergence method. The droplet's instantaneous temperature $T_{R,I}$ is defined and made equal to the temperature $T_{R,I,it=IT}$ selected for the final iteration IT of the iteration cycle:

$$I=2\rightarrow I_f:\ \ T_{R,I,it}\ \leftrightarrow T_{J,I,it}\rightarrow it=1\rightarrow IT;\ T_{R,I}=T_{J,I,it=IT}, \tag{14a}$$

$$\left[1-\frac{\lambda_{ef,I,it=IT}\left.\frac{\partial T(r,\tau)}{\partial r}\right|_{r=R_{I,it=IT}}+m_{v,I,it=IT}L_{l,I,it=IT}}{\lambda_{vg,I,i=IT}\frac{T_g-T_{J,I,it=IT}}{2R_{I,IT-1}}\mathrm{Nu}_{f,I,it=IT}}\right]\times 100\,{}^{o}\!/_{o}<\delta_{IT}=0.05\,{}^{o}\!/_{o}\,, \tag{14b}$$

$$\lambda_{vg,I,it=IT}\equiv\ \lambda_{vg}\left(T_{vg},X_{v,vg}\right), \tag{14c}$$

$$T_{vg}=T_{J,I,it=IT}+\frac{1}{3}\left(T_g-T_{J,I,it=IT}\right);X_{v,vg}=X_{v,J,I,it=IT}+\frac{1}{3}\left(X_{v,g}-X_{v,J,I,it=IT}\right). \tag{14d}$$

During simulation of the technological droplet's phase changes, it was controlled that each iterative (13) cycle would require equation (14b). The example of such control is provided in Fig. 1a. Figure 1b presents examples of the iterative cycle.

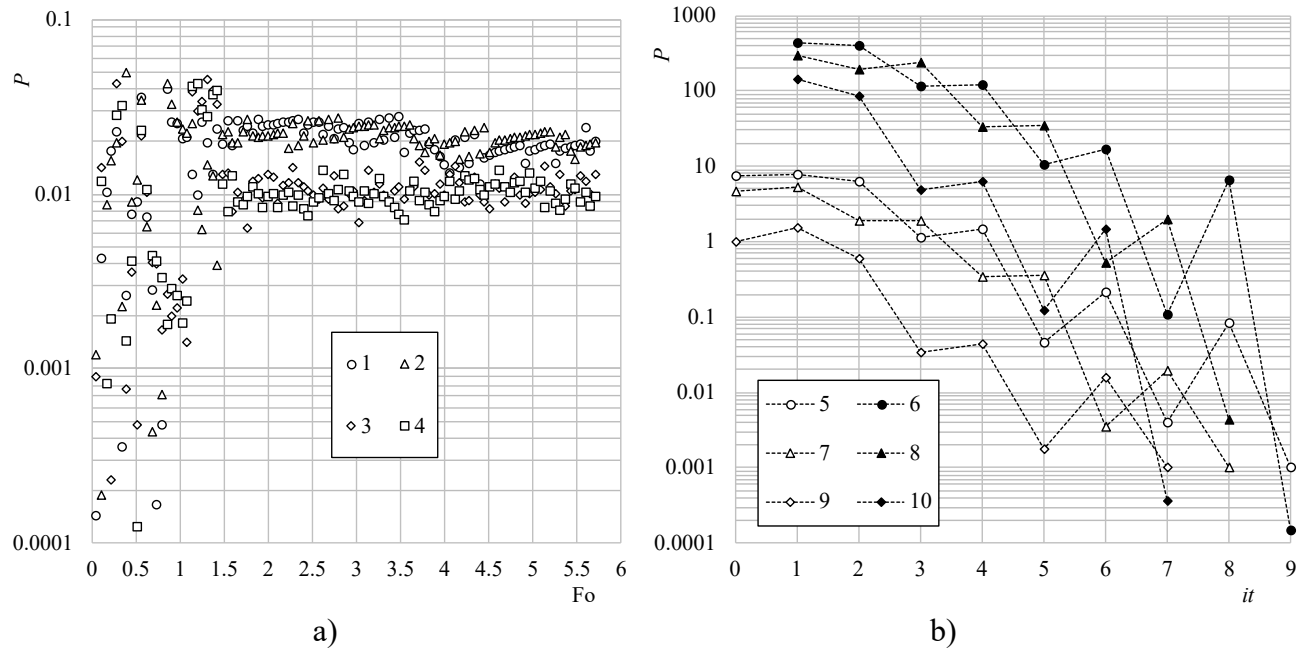

Fig. 1. Examples of convergence control (a) and course (b) of the iterative cycle (13). Boundary conditions:(1, 3, 5-10) combined heating; (2, 4) convective heating; t_g,ºC: (1, 2, 5-10) 100, (3, 4) 150; p_b=0.1 MPa; $X_{v,g}$=0.2; $t_{l,0}$=40ºC; $R_{l,0}$=250 μm; Re_0=100; Fo: (5, 6) 0.057, (7,8) 0.114, (9, 10) 0.343. Meaning of parameter P: (5, 7, 9) $P=\left|t_{i,J,it}-t_{i,J,IT}\right|+0.001$ºC, (1-4, 6, 8, 10) $P=|\delta_{it}|$%.

3. Results and discussion

A detailed numerical investigation was conducted of the phase changes in technological water droplets at the range of temperatures characteristic of the technologies applied in wet flue gas condensing economizers. The possible influence of radiation was also evaluated. The external radiation source was assumed to be the soot covered walls that restrict the flue gas flow. The experimental droplets were treated as large water droplets, when their diameter was in the order of one millimeter. The technological droplets were considered as medium, when their diameter was in the order of several hundred micrometers, and as small, when their diameter was in the order of several tens of microns.

3.1. The Fourier time scale and its advantages

It was convenient to use an identical Reynolds number Re_l for the definition of the boundary conditions of convective heat and mass transfer processes of droplets with different dispersity; however, even in this case, the heating of technological droplets of different dispersity differed significantly (Fig. 2a). The condensing economizer technology typically applies a fairly wide range of boundary conditions concerning flue gas temperature and humidity (tg≡40→250ºC; $X_{v,g}$≡0.07→0.4), and, therefore, extensive numerical research would be necessary in order to conduct a thorough investigation of the cycle of phase change regimes in sprayed water droplets (2 a) in respect of droplet dispersity. Hence, the numerical research was optimized based on the assumption that in the case of convective heating, the droplet heating becomes universal concerning dispersity (Fig. 2b) in the time scale of the Fourier number (the Reynolds number Re_l must be identical for the droplets).

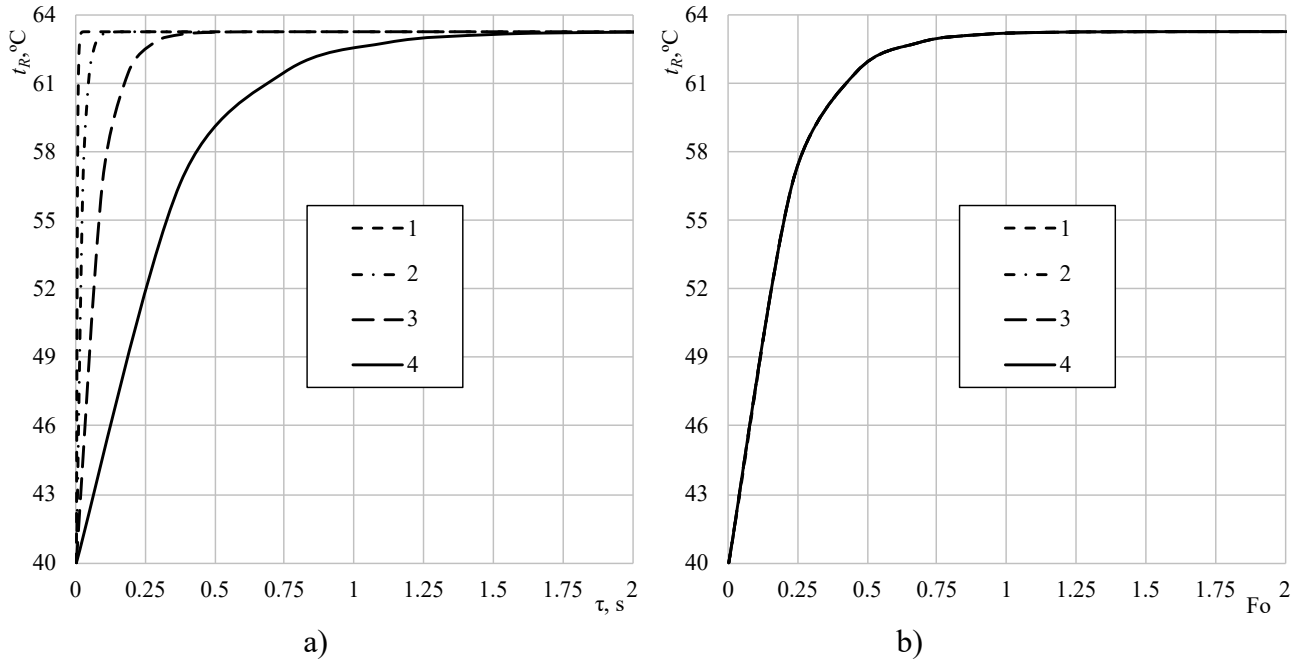

Fig. 2. The heating of water droplets of different dispersity in the transitional phase change regime in humid air flow in the timescale (a) and in the timescale of the Fourier number (17) (b), when t_g=130ºC; p_b=1013.25 hPa; $t_{l,0}$=40ºC; Re_0=125; $2R_0$, μm: (1) 100, (2) 250, (3) 500, (4) 1000.

It is easy to transform the real timescale into a timescale of the modified Fourier number:

$$\tau \equiv 0 \rightarrow \tau_{co} \rightarrow \tau_r \rightarrow \tau_e \rightarrow \tau_f;\ \mathrm{Fo} = \frac{a_{l,0}}{R_0^2}\tau;\ \mathrm{Fo} \equiv\ 0 \rightarrow \mathrm{Fo}_{co} \rightarrow \mathrm{Fo}_e \rightarrow \mathrm{Fo}_f \qquad (15)$$

Thus, the graph of the temporal function $t_R(\tau)$ defining the temperature variation on the surface of technological droplets of different dispersity is specific (Fig. 2a), while the graph of function t_R(Fo) in the timescale of the Fourier number becomes universal in respect of droplet dispersity (Fig. 2b). The convenience of using the timescale of the Fourier number becomes obvious during the graphical interpretation of dimensionless functions P_f(Fo)/$P_{f,0}$ of P_f parameters of phase changes in technological droplets. A good illustration is provided in Fig. 3 which presents an example of the change in diameter of technological droplets in the cycle of phase change regimes (15). The change in diameter of different dispersity droplets in the cycle of phase change regimes (2a) is defined by specific graphs of the temporal function $R(\tau)$ (Fig. 3a). However, the graph of the rational function R(Fo)/R_0 in the cycle of phase change regimes (15) is universal in respect of droplet dispersity (Fig. 3b). All graphs of the dimensionless functions P(Fo)/P_0 of heat and mass transfer parameters will be universal in respect of droplet dispersity in the cycle of phase change regimes (15), when the Reynolds number of the technological droplets is identical. It goes without saying that the temperature and humidity of the gas flow must be defined and the initial droplet temperature must be the same.

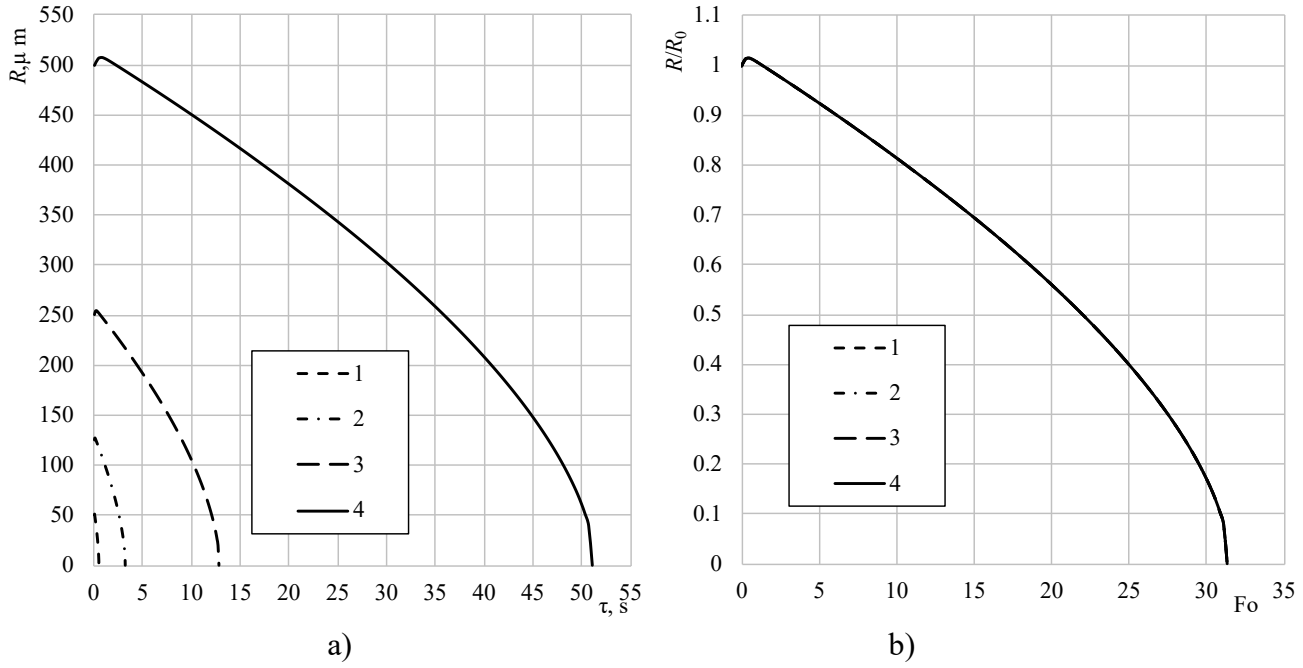

Fig. 3. The dynamics of water droplets of different dispersity in wet air flow in the timescale (a) and in the timescale of the Fourier number (b), when t_g=130ºC; p_b=1013.25 hPa; $t_{l,0}$=40ºC; Re_0=125; $2R_0$, μm: (1) 100, (2) 250, (3) 500, (4) 1000.

3.2 Validation of numerical simulation methodology

The methodology of the numerical simulation of the technological droplet's heat and mass transfer was validated for the cases of convective and combined heating. At first, the boundary conditions used in the experiments [28] were recreated numerically. In order to simulate the external convective transfer of the technological droplet, the same boundary conditions as in the experiments [28] were used, based on the initial water temperature, and the air flow temperature and humidity, and the experimental Reynolds number $Re_{l,0}$ was also applied. A certain discrepancy between the model of internal heat transfer of the droplet and the experimental conditions remained since it is very difficult to repeat the experimental conditions of internal heat transfer according to the homogenized droplet model described in Subchapter 2.1. Because of the strict assessment of the research applied, a composite two-layered model of the droplet's heat and mass transfer would be necessary. The development of such a model would require additional mathematical analysis and correction of the digital algorithm for heat and mass transfer of a droplet in the "LASAS" software. In addition, the volume of the article would increase

significantly. In order to avoid this, the temperature gradient of the technological droplet was defined according to the model of a homogeneous sphere where its initial diameter equals the diameter $2R_{lm,0}$ of the experimental droplet.

The graphs of simulated functions $t_{l,m}$(Fo) that describe the heating of the technological droplet are specific; there are clear variations in transitional phase change regimes and leveling-off in the equilibrium evaporation regime (curves in Fig. 4). The temperature $t_{l,e}$ that defines the simulated thermal state of equilibrium evaporation of the technological droplet matches the experimental temperature $t_{wb,eks}$ within a tolerance of 2 ºC (points in Fig. 4). The temperature $t_{wb,eks}$ of the wet-bulb thermometer congruous with the boundary conditions of the experimental droplet heat and mass transfer is defined according to the algorithm:

$$t_{g,eks},\ X_{v,g,eks},\ p_b \rightarrow p_{v,s} = p_s\left(t_{g,eks}\right);\ p_{v,g} = X_{v,g,eks}p_b \rightarrow \varphi_{g,eks} = \frac{p_{v,g}}{p_{v,s}}100\ ^o/_o$$

$$\varphi_{g,eks},\ t_{g,eks} \rightarrow t_{wb,eks}\ [35] \qquad (16)$$

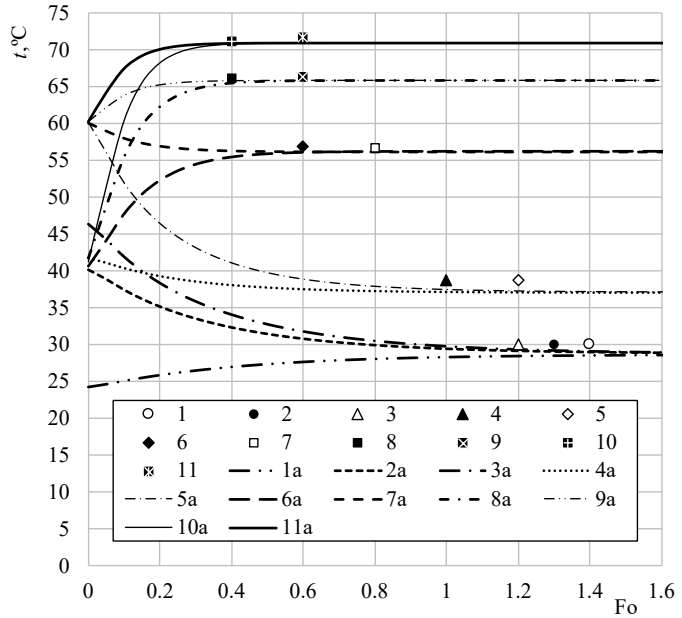

Fig. 4. The dynamics of water droplet heating in the time scale of the Fourier number simulated at the boundary conditions of the experiments [28]. Meaning of the parameter t: $t=t_{l,m}$ for curves; $t=t_{wb,eks}$ for points. t_g,ºC: (1) 80.6, (2) 81.2, (3) 81.1, (4) 132.1, (5) 132.7, (6) 130.2, (7) 128.5, (8) 132.1, (9) 132.6, (10) 130.1, (11) 129.5; X_v: (1-5) 0.01, (6,7) 0.128, (8, 9) 0.226, (10, 11) 0.3; $t_{l,0}$,ºC: (1) 24.3, (2) 40.2, (3) 46.4, (4) 41.8, (5) 60.3, (6) 40.7, (7) 60.1, (8) 41.8, (9, 11) 60.3, (10) 41.3; $2R_m$, mm: (1) 1.775, (2) 1.787, (3) 1.453, (4) 1.765, (5) 1.665, (6) 2.122, (7) 2.138, (8) 2.09, (9) 2.336, (10) 2.364, (11) 2.052; Re: (1) 134, (2) 133.1, (3) 117.7, (4) 126, (5) 121, (6) 164.5, (7) 167.7, (8) 172.5, (9) 200.1, (10) 217.4, (11) 192.8.

For other cases of the boundary heat and mass transfer conditions (not the experimental investigation), the initial temperature of the technological droplets was set to match the 40 ºC temperature of vapor condensate that is widely applied in the biofuel incineration technology. Convective heat and mass transfer in the technological droplet is the predominant case when water is sprayed into the condensing economizer to the flue gas with a temperature lower than 100 ºC. For this case, the numerical simulation methodology was validated by comparing the simulated thermal state of the technological droplet to the temperature t_{wb} of the wet-bulb thermometer in the flow of defined temperature and relative humidity air (Fig. 5) (temperature t_{wb} was defined according to respective air parameters according to data in [36]). In all simulated cases, at the end of the transitional evaporation regime, the technological droplets reached the calculated temperature $t_{l,e}$ characteristic of equilibrium evaporation. The droplet heated up (Fig. 5, curves 4–8) or cooled down (Fig. 5, curves 1–3) to the

temperature $t_{l,e}$. The reliability of the applied methodology for the simulation of the technological droplet's heat and mass transfer is justified in the case of convective heating because the temperature $t_{l,e}$ calculated in a wide range of atmospheric air flow temperatures t_a and relative humidity practically matches the temperature t_{wb} of the wet-bulb thermometer defined according to corresponding air parameters [36].

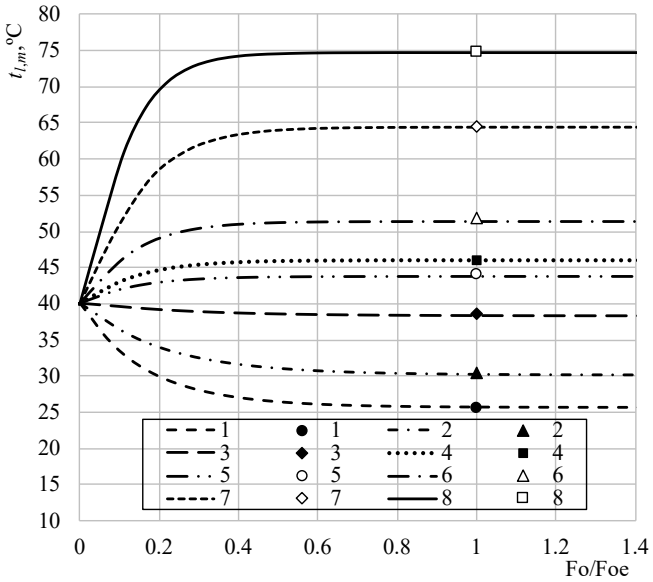

Fig. 5. The influence of atmospheric air temperature and relative humidity on the dynamics of water droplet heating. t_g,ºC: (1-4) 50, (6-8) 80; φ, %: (1, 5) 15, (2, 6) 25, (3, 7) 50, (4, 8) 80; p_b=1013.25 hPa; $t_{l,0}$=40ºC; Re=100; 2R=200 μm. The points correspond to the respective t_{wb} temperature of the wet-bulb thermometer defined according to the atmospheric air temperature and relative humidity [36].

The phase change processes at the surface of technological droplets and defined by the vapor flux g_v [kg/s] condition the effectiveness of water injection. When the flue gas temperature is higher than 100 ºC, the phase change processes in the sprayed water take place when the droplets are heated by convection and radiation. The radiation is caused by the flue gas and the surfaces restricting the flue gas flow. Because of the multiple light beam reflection and because the surfaces are covered in soot, the intensity of radiation falling on the droplet is close to the intensity of blackbody radiation. The vapor flux at the surface of the technological droplet changes in the transitional phase change regime and reaches the value of $g_{v,e}$ characteristic of equilibrium evaporation. The value of $g_{v,e}$ is defined experimentally in [23] when water droplet ($R \equiv 0.5–1.6$ *mm*) undergoes equilibrium evaporation in the air of high temperature ($t_g \equiv 405–860$ *ºC*) under combined heating conditions. The same boundary conditions as in these experiments were set in the numerical simulation performed according to the methodology described in Chapter 2; however, the droplet's diameter was set to always remain constant in phase change regimes (as was done in the experiments of [23]). The g_v(Fo) functions describing the dynamics of the vapor flux at the surface of the droplet were defined numerically in a wide range of varying boundary conditions. The graphs of these functions clearly show (lines in Fig. 6) that the vapor flux increases rapidly at the initial stage of transitional evaporation and consistently stabilizes at the final stage and defines the vapor flux $g_{v,e}$ characteristic as transitional evaporation. The vapor flux does not vary in the equilibrium evaporation regime because the droplet's diameter is artificially kept constant.

The equilibrium evaporation vapor flux $g_{v,e}$ defined by the g_v(Fo) functions calculated in wide ranges of varying temperature t_w=t_g of the radiation source and droplet dispersity is in good correlation (Fig. 6) with the experimental [23] data (defined by an accuracy of five percent, as stated by the authors). This justifies the credibility of the applied droplet heat and mass transfer simulation

methodology in the case of combined heating.

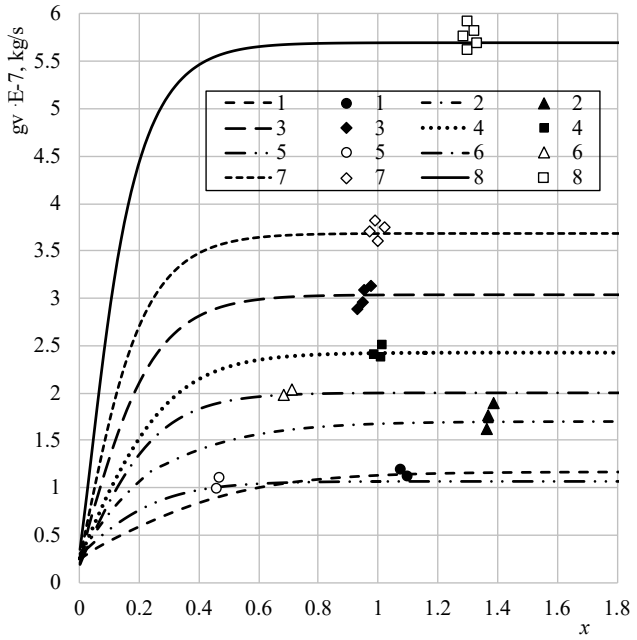

Fig. 6. The influence of the water droplet size and air temperature on the evaporation rate of a droplet in the case of combined heating. Points are data [23]. Lines are results of numerical simulations. t_g,ºC: (1, 2) 405, (3) 708, (4) 616, (5-8); 738; R(Fo)=const, [mm]: (1) 1.08, (2) 1.38, (3) 0.95, (4, 7) 1, (5) 0.7, (8)1.3; p_b=0.1 MPa; $t_{l,0}$=40ºC; w_{lg}=0.01 m/s. The meaning of the x-coordinate of the abscissa: x≡R [mm] for points, x≡Fo for lines.

3.3. Phase changes of the technological droplet in biofuel exhaust gas flow

The calculated mass temperature $t_{l,\mathrm{m}}$ of the technological water droplet (hereafter "droplet") heated by biofuel flue gas through convection is changing in the transitional phase change regime until the droplet reaches (heats up or cools down) the thermal state that is characteristic of equilibrium evaporation and is defined by the temperature $t_{l,e}$ (Fig. 3).

The qualitative change in the droplet's thermal state (heating up or cooling down) can be defined by the relation between the equilibrium evaporation temperature t_e and the droplet's initial temperature $t_{l,0}$: when t_e>$t_{l,0}$, the droplet heats up; when $t_{l,e}$<$t_{l,0}$, the droplet cools down. The uniqueness of the change in the droplet's thermal state is obvious in the dynamics of the temperature field gradient (Fig. 7a). In the transitional phase change regime, a temperature field with a positive gradient forms in the droplet that is heated up (Fig. 7a, curves 1, 6, 9 and 11) and a temperature field with a negative gradient in the droplet that is cooled down (Fig. 7a, curves 2, 4, 5 and 7). Extreme values of the temperature gradient are recorded in heating as well as in cooling droplets, while in the equilibrium evaporation regime the temperature gradient equals zero (Fig. 7a). The change in the droplet's thermal state is closely connected with the phase changes at the droplet's surface that are defined by the dynamics of the vapor flux (Fig. 7b). The condensation regime takes place when the droplet's temperature is lower than the dew point temperature (the regime is identified by a calculated negative vapor flux (Fig. 7b, curves 6, 9 and 11). The heat emitted during phase changes in the condensation process speeds up the heating of the droplet and allows the formation of an instantaneous temperature field of the positive gradient of almost 25 000 K/m in the droplet (Fig. 7a, curve 10). The calculated highest negative gradient in the cooling droplet was almost 14 000 K/m (Fig. 7a, curve 5).

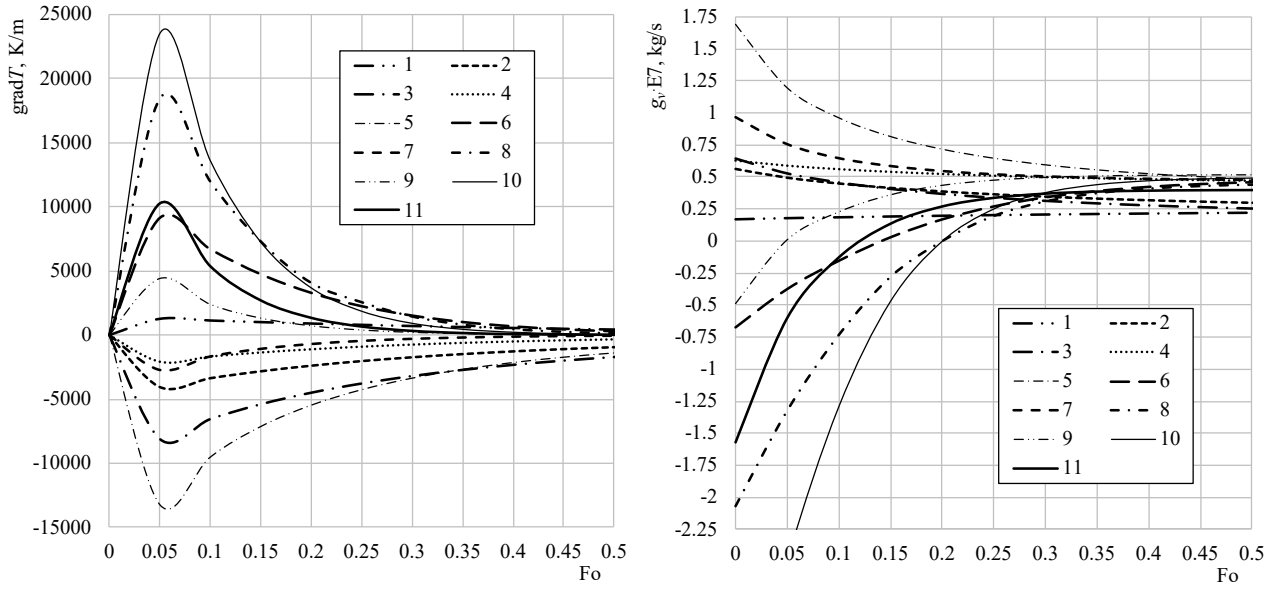

a) b)

Fig. 7. The dynamics of the temperature gradient (a) and vapor flux (b) of the water droplet in the case of convective heating. The parameter a/R^2, s^{-1}: (1) 30.02, (2) 30.14, (4) 38.69, (5) 38.75, (6) 56.86, (7) 56.75, (9) 66.25, (11) 71.18. Boundary conditions as in Fig. 4.

The dynamics at the surface of the droplet of vapor flux define the change of the droplet's geometrical dimension (diameter, volume and surface area) in the cycle of the phase change regime. In the transitional phase change regime, the graph of the calculated function S(Fo) describing the change at the droplet's surface depends on the boundary heat and mass transfer conditions in the droplet (the graphs of S(Fo) functions are different when the droplet heats up in a low humidity flue gas (Fig. 8a) and when it heats up in a higher humidity flue gas (Fig. 8b)).

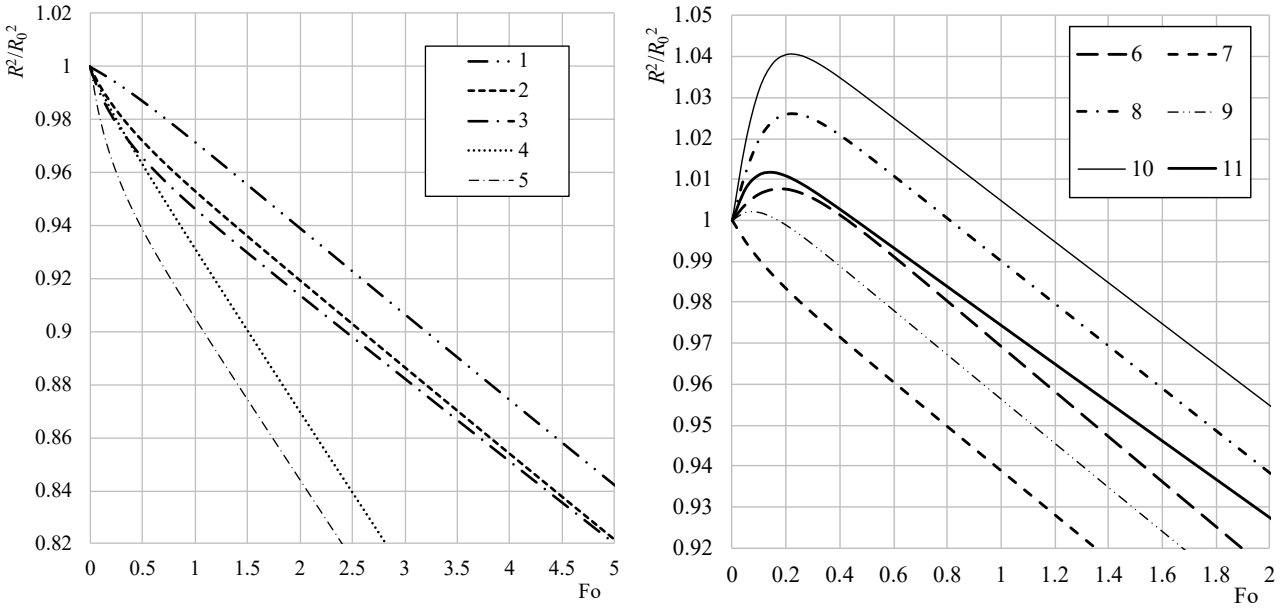

a) b)

Fig. 8. The dynamics of the dimensionless surface area S/S_0 of the technological droplet heated by convection. Boundary conditions as in Fig. 4.

In the case of convective heating, the surface area of a technological droplet decreases linearly during the equilibrium evaporation regime (Fig. 8). This is also confirmed experimentally [28] and is

known as the D^2 law [37]. The change of the geometrical dimension of the technological droplet in the transient phase change regimes is determined by the initial water temperature and the humidity of the gas flow. This is also confirmed experimentally [28]. Hence, the calculated dynamics of the geometrical dimension of the technological droplet fully correspond to the regularities of the experimental droplet.

The boundary conditions of heat and mass transfer in water droplets sprayed during the process of heat recovery from an exhaust gas change when the flue gas cools down, becomes more humid (because of water sprayed before the recuperative type condensing heat exchanger) or dries up (because of water sprayed into the contact type condensing shell and tube heat exchangers). When water is sprayed into an exhaust gas flow of higher temperature, the phase change processes take place when the droplets are under the influence of combined heating. The dispersity of the droplets defines the process of radiation absorption in water droplets (Fig. 9). Smaller water droplets absorb radiation flux in the central layers (Fig. 9, curves 1–3), while larger droplets absorb the flux in external layers (Fig. 9, curves 6, 7). The droplet size changes during phase changes: the droplet grows in the condensation regime and consistently decreases during evaporation. During phase changes, the technological droplets become as if more transparent and go through all radiation absorption cases presented in Figure 9. Hence, the initial dispersity of the droplets is very important when considering the change in their thermal state in the transitional phase change regime. Under the influence of radiation, the heating of central layers of smaller droplets becomes faster, while the faster heating of external layers of bigger droplets allows the surfaces of the droplets to reach the dew point temperature. This has a direct influence on the possible change of transitional phase change regimes.

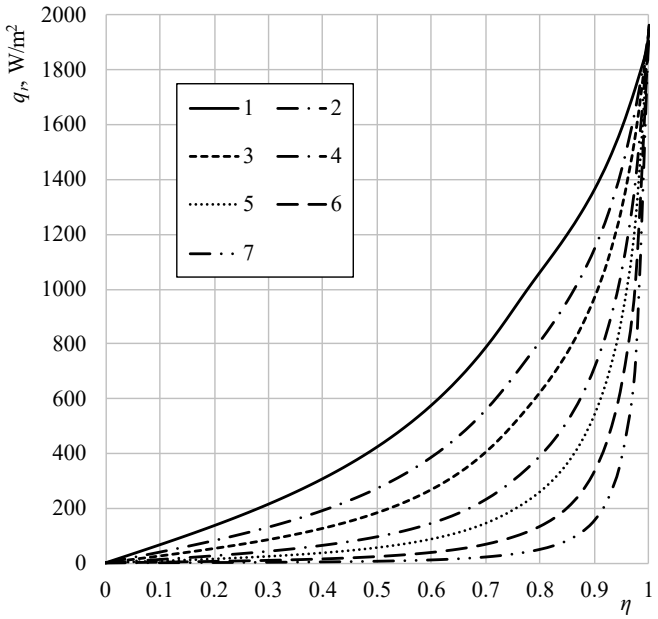

Fig. 9. The influence of droplet dispersity on absorbed radiation flux when $t_w=t_g$=200ºC; t_l=40ºC; R, μm: (1) 50, (2) 75, (3) 100, (4); 150, (5) 200, (6) 300, (7) 500.

The radiation flux from an external source will be defined by the flue gas temperature. In order to define the possible radiation influence on phase changes of water droplets sprayed into a condensing economizer, phase changes of a large droplet of 500 micrometers in diameter were simulated in the flue gas flow of different temperatures (t_g≡100–250 ºC) and medium humidity level $X_{v,g}$=0.2 in the cases of convective heating and combined heating (Fig. 10). The heating method of the droplet had no influence on the dynamics of vapor flux in the condensation regime. However, when the temperature of flue gas increased from 100 ºC to 250 ºC, the duration of the condensation regime shortened by nearly a factor of two (Figure 10, curves 1 and 4). In the transitional evaporation regime, the heating method of the droplet becomes influential (this is illustrated by consistently increasing the separation of dashed and solid curves; the separation settles in the equilibrium evaporation regime (Fig. 10, curves 3 and 4).

However, the influence of radiation on phase changes of technological droplets can be denied when water is sprayed into the flue gas of a lower temperature than 150 ºC (Fig. 10, curves 1, 2).

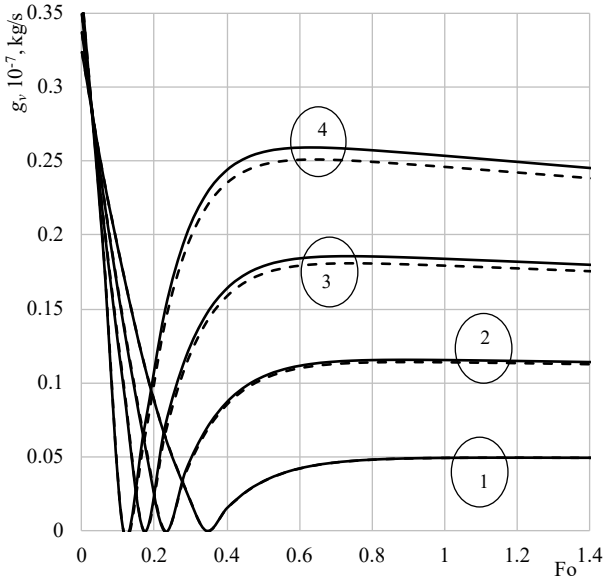

Fig. 10. The influence of flue gas' temperature on the calculated vapor flux in phase change regimes of the technological droplet in cases of combined (solid lines) and convective (dashed lines) heating. t_l=40ºC; R_0=250 μm; Re_0=100; $X_{v,g}$=0.2: t_g,ºC: (1) 100, (2) 150, (3) 200, (4); 250.

Before the flue gas is directed to a condensing economizer, it is cooled down and additionally humidified with sprayed water (water vapor mass fraction can increase up to $X_{v,g}$=0.5) so as to additionally clean it from solid particles and efficiently recover heat by complete vapor condensation. In the condensing economizer, the flue gas dries when water vapor condenses. In order to define the influence of flue gas humidity on the phase changes of the water sprayed into the condensing economizer, the transitional phase change regime of a technological droplet of medium diameter of 200 micrometers with initial water temperature of 40 ºC was simulated in a flue gas of 100 ºC when $X_{v,g}$=0.1→0.5. The condensing vapor flux of phase changes clearly depends on the humidity of the flue gas and varies from 0.03E-7 kg/s to 0.6 kg/s (Fig. 11). The volume of the droplet increases quickly because of the condensate (Fig. 12a). The increase in the condensation regime clearly depends on the humidity of the flue gas, and the volume of the droplet can increase by up to almost ten percent in an additionally humidified flue gas (Fig. 12a, curve 6). However, the condensation process slows down sharply (Fig. 11) as the droplet heats up (Fig. 12b). In contact type condensing shell and tube exchangers, favorable conditions exist for sprayed water droplets to rapidly reach the dew point temperature (Fig. 12b). Hence, when recovering heat from an exhaust gas in the contact type condensing shell and tube exchanger, the temperature on the surface of droplets must be controlled so it does not exceed the dew point temperature. Then, when the transitional evaporation regime starts again, the flue gas is to be humidified.

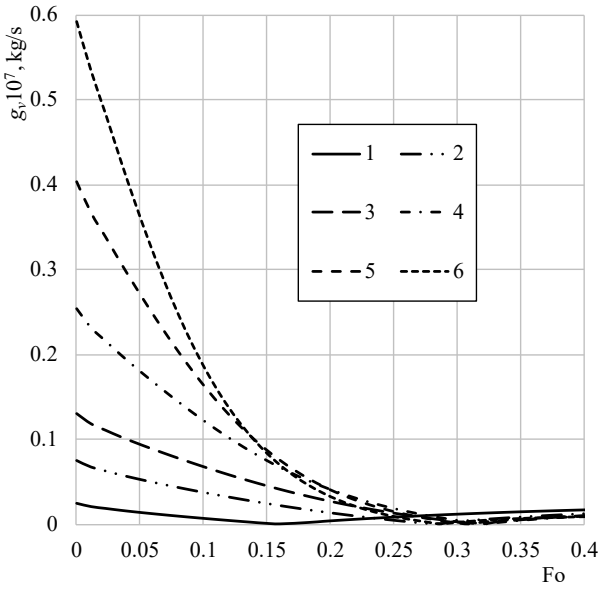

Fig. 11. The influence of flue gas' humidity on the calculated vapor flux in phase change regimes of the technological droplet in the condensing economizer. t_l=40ºC; R_0=100 μm; Re_0=100; t_g=100ºC; $X_{v,g}$: (1) 0.1, (2) 0.15, (3) 0.2, (4) 0.3, (5) 0.4, (6) 0.5.

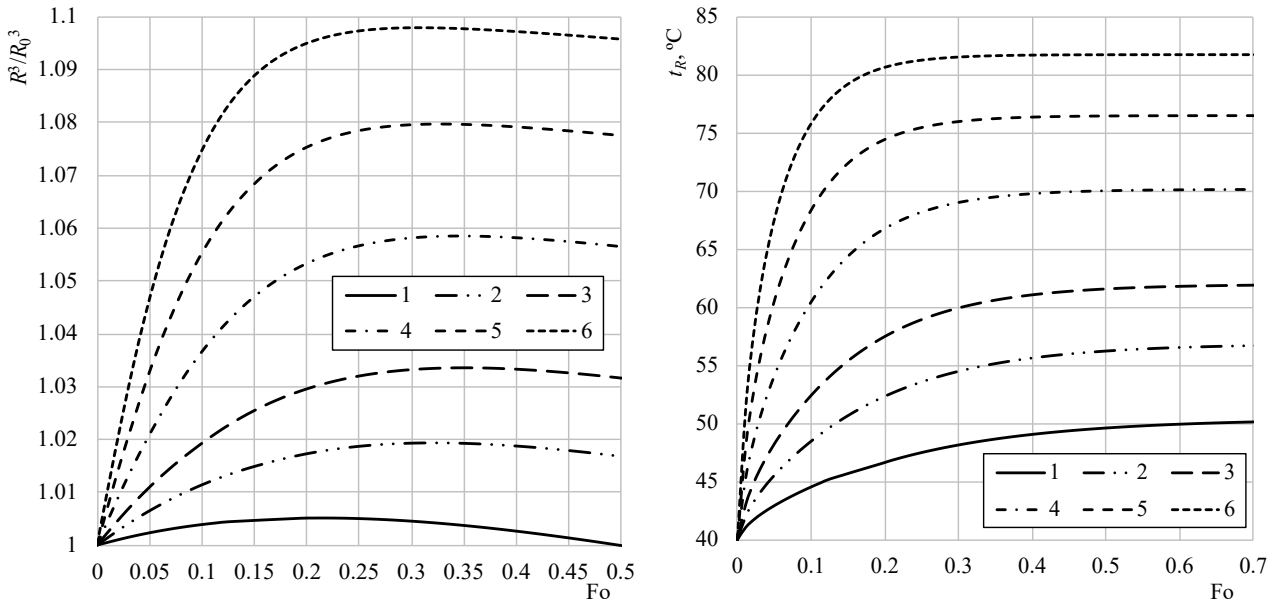

a) b)

Fig. 12. The dependence of the growth (a) and heating (b) of the technological droplet in the condensing economizer on the humidity of the flue gas flow. t_l=40ºC; R_0=100 μm; Re_0=100; t_g=100ºC; $X_{v,g}$: (1) 0.1, (2) 0.15, (3) 0.2, (4) 0.3, (5) 0.4, (6) 0.5.

4. Conclusions

The following conclusions were drawn after the numerical simulation of phase changes of water droplets in wet flue gas flow:

1. The reliability of the provided methodology of heat and mass transfer of water droplets is confirmed by the good compatibility of the modeling results with the experimental data in the cases of convective and combined heating of droplets.
2. The results of the numerical modeling demonstrated the essential influence of the humidification of air on the cycle of phase change regimes of water droplets.

3. The numerical simulation proved that the influence of radiation can be ignored when modeling combined heat and mass transfer processes in water sprayed into condensing economizers if the temperature of exhaust gas is lower than 150 ºC.
4. The numerical simulation defined that there is a close correlation between the variation in phase change regimes in the droplets of water sprayed into biofuel flue gas and the dynamics of the temperature on the droplet's surface. Factors determining the change in the droplet's thermal state are the temperature of sprayed water and droplet dispersity.
5. In order to cool down biofuel flue gas rapidly and additionally humidify it effectively before the condensing economizer, the water must be sprayed when the $t_{l,0} > t_{l,e}$ condition is valid as this will cause the droplets to cool down and evaporate intensively.
6. In a contact type condensing economizer, the process of heat recovery from flue gas will be efficient when the condition of technological water spraying $t_l << t_{dp}$ is valid.

References

1. Sirignano WA, Mehring C. Review of theory of distortion and disintegration of liquid streams. Prog Energy Combust Science, 2000; 26: 609-655. https://doi.org/10.1016/S0360-1285(00)00014-9
2. Alnaimat F. Heat transfer analysis of air-mist evaporative cooling in heat sink. Int J Thermofluids, 2022; 14: 100145. https://doi.org/10.1016/j.ijft.2022.100145
3. Men Y, Liu X, Zhang T. Analytical solutions of heat and mass transfer process in combined gas – water heat exchanger applied for waster heat recovery. Energy, 2020; 206: 118095. https://doi.org/10.1016/j.energy.2020.118095
4. Carton JG, Lawlor V, Olabi AG, Hochenauer C, Zauner G. A Water droplet accumulation and motion in PEM (Proton Exchange Membrane) fuel cell mini channels. Energy, 2012; 39: 63-73. https://doi.org/10.1016/j.energy.2019.116488
5. Miliauskas G, Maziukienė M, Jouhara H, Poškas R. Investigation of mass and heat transfer transitional processes of water droplets in wet gas flow in the framework of energy recovery technologies for biofuel combustion and flue gas removal. Energy, 2019; 173: 740-754. https://doi.org/10.1016/j.energy.2019.02.101
6. Ijaodola OS, El-Hassan Z, Ogungbemi E, Khatib FN, Wilberforce T, Thompson J, Olabi AG. Energy efficiency improvements by investigating the water flooding management on proton exchange membrane fuel cell (PEMFC). Energy, 2019; 179: 246-267. https://doi.org/10.1016/j.energy.2019.04.074
7. Fuchs NA. Evaporation and droplet growth in gaseous media. 1959; London: Pergamon Press.
8. Perez JG, Leclaire S, Ammar S, Trepanier JY, Reggio M, Benmeddour A. Investigations of water droplet impact and freezing on a cold subatrate with the Lattice Boltzmann method. Int J Thermofluids, 2021; 12: 100109. https://doi.org/10.1016/j.ijft.2021.100109
9. Sazhin SS. Droplets and Sprays. 2014; Springer, Heidelberg. https://doi.org/10.1007/978-1-4471-6386-2
10. Sirignano WA. Fluid Dynamics and Transport of Droplets and Sprays. 2000; Cambridge University Press. https://doi.org/10.1017/CBO9780511529566
11. Miliauskas G. Interaction of the transfer processes in semitransparent liquid droplets. Int J Heat Mass Trans, 2003; 46: 4119-4138. https://doi:10.1016/S0017-9310(03)00231-X
12. Siegel R, Howell JR. Thermal Heat Transfer. 1972; New York: McGraw-Hill.
13. Hale GM., Querry MR. Optical constant of water in the 200-nm to 200-μm wavelength region. Aplied Optics, 1973; 12: 555-562.
14. Tseng CC., Viskanta R. Enhancement of water droplet evaporation by radiation absorption. Fire Safety J, 2006; 41: 236–247. https://doi.org/10.1016/j.firesaf.2006.01.001
15. Dombrovsky LA, Levashov VY, Kryukov AP, Dembele S, Wen JX. A comparative analysis of shielding of thermal radiation of fires using mist curtains containing droplets of pure water or sea water. Int J Thermal Sc, 2020; 152: 106299. https://doi.org/10.1016/j.ijthermalsci.2020.106299

16. Miliauskas G, Ramanauskas V, Maziukienė M. The interaction of the complex transfer processes in the phase transformations regimes of a water droplets. Int J Heat Mass Trans, 2021; 169: 120761. https://doi.org/10.1016/j.ijheatmasstransfer.2020.120761
17. Sirignano WA. Advances in droplet array combustion theory and modeling. Prog Energy Comb Sc Transfer, 2014; 42: 54-86. https://doi.org/10.1016/j.pecs.2014.01.002
18. Brewster M, Li X. Analysis of radiation-induced cooling and growth of mist and cloud droplets. Int J Heat Mass Trans, 2021; 166: 120674 https://doi.org/10.1016/j.ijheatmasstransfer.2020.120674
19. Piskunov M, Strizhak P, Volkov R. Experimental and numerical studies on the temperature in a pendant water droplet heated in the hot air. Int J Thermal Sc, 2021; 163: 106855. https://doi.org/10.1016/j.ijthermalsci.2021.106855
20. Dombrovsky LA, Fedorets A, Levashov VY, Kryukov AP, Bormashenko E, Nosonovsky M. Stable cluster of identical water droplets formed under the infrared irradiation: Experimental study and theoretical modeling. Int J Heat Mass Transfer, 2020; 161: 120255. https://doi.org/10.1016/j.ijheatmasstransfer.2020.120255
21. Zhang Y, Huang R, Zhou P, Huang S, Zhang G, Hua Y, Qian Y. Numerical study on the effects of experimental parameters on evaporation characteristic of a droplet. Fuel, 2020; 161: 120255. https://doi.org/10.1016/j.fuel.2021.120323
22. Strizhak PA, Volkov RS, Antonov DV, Castanet G, Sazhin SS. Application of the laser induced phosphorescence method to the analysis of temperature distribution in heated and evaporating droplets. Int J Heat Mass Transfer, 2020; 163: 120421. https://doi.org/10.1016/j.ijheatmasstransfer.2020.120421
23. Ivanov M, Smirnova EV. Experimental research of liquid droplets evaporation velocity in non-moving high temperature environment. Trans. IGI, 1962; 19: 46–58.
24. Vakkilainen EK. 2 - Solid Biofuels and Combustion. Steam Generation from Biomass / Construction and Design of large Boilers, 2020; 93: 2409-2414. https://doi.org/10.1016/B978-0-12-804389-9.00002-2
25. Malaťák J, Gendek A, Aniszewska M, Velebil J. Emissions from combustion of renewable solid biofuels from coniferous tree cones. Fuel, 2020; 276: 118001. https://doi.org/10.1016/j.fuel.2020.118001
26. Kruczek HP, Ostrycharczyk M, Zgóra J. Co-combustion of liquid biofuels in PC boilers of 200 MW utility unit. Proc Combustion Institute, 2013; 34: 2769-2777. https://doi.org/10.1016/j.proci.2012.08.010
27. Rodríguez JL., Alvarez X, Valero E, Ortiz L, Rodríguez NT, Alonso CA. Design of solid biofuels blends to minimize the risk of sintering in biomass boilers. J Energy Institute, 2020; 93: 2409-2414. https://doi.org/10.1016/j.joei.2020.07.015
28. Miliauskas G, Puida E, Poškas R, Ragaišis V, Paukštaitis L, Jouhara H, Mingilaitė L. Experimental investigations of water droplet transient phase changes in flue gas flow in the range of temperatures characteristic of condensing economizer technologies. 2022. In Press.
29. Moreira ALN, Moita AS, Panao MR. Advances and challenges in explaining fuel spray impingement: How much of single droplet impact research is useful? Prog Energy Combust Sc, 2010; 36: 554-580. https://doi.org/10.1016/j.pecs.2010.01.002
30. Bennen G. Droplet Collision, 2011; In ASHGRIZ, N.Sud. Handbook of Atomization and Sprays. Boston, MA: Springer US.
31. Miliauskas G. Regularities of unsteady radiative-conductive heat transfer in evaporating semitransparent liquid droplet. Int J Heat Mass Transfer, 2001; 44: 785-798. https://doi.org/10.1016/S0017-9310(00)00127-7
32. Abramzon B, Sirignano WA. Droplet vaporization model for spray combustion calculations. Int J Heat Mass Transfer, 1989; 32: 1605-1618. https://doi.org/10.1016/0017-9310(89)90043-4
33. Clift R, Grace JR, Weber ME. Bubbles, Drops and Particles. 1978; New York: Academic Press.
34. Renksizbulut M, Yuen MC. Numerical study of droplet evaporation in a high temperature stream. J Heat Transfer, 1983; 105: 388-394

35. Miliauskas G, Adomavičius A, Maziukienė M. Modelling of water droplets heat and mass transfer in the course of phase transitions. II: Peculiarities of the droplet radial coordinate and the time grid calibration. Nonlinear Analysis: Model Control, 2017; 2: 135-151. https://doi.org/10.15388/NA.2017.3.7.
36. http://www.flycarpet.net/en/PsyOnline
37. Elperin T, Krasovitov B. Radiation, thermal diffusion and kinetic effect in evaporation and combustion of large and moderate size fuel droplets. Int J Heat Mass Transfer, 1995; 38: 409-418. https://doi.org/10.1016/0017-9310(94)00168-U

Declaration of interest

Conflicts of interest: none

Funding

This research was funded by Research Council of Lithuania (LMTLT), grant number S-MIP-20-30.